SOILS AND FOUNDATIONS Vol. 42, No. 5, 27-36, October 2002
Japanese Geotechnical Society

OBSERVATION OF GRAIN MOTION IN THE INTERIOR OF A PSC TEST SPECIMEN BY LASER-AIDED TOMOGRAPHY

TAKASHI MATSUSHIMA[i], TAKAYUKI ISHII[ii] and KAZUO KONAGAI[iii]

ABSTRACT

This paper presents a Laser-Aided Tomography/plane strain compression (LAT/PSC) testing method, a new PSC test allowing for a discussion of granular micromechanics with visualized granular fabrics. LAT technique is utilized to visualize in real time any arbitrary cross-section of a granular specimen. An image processing algorithm, suited for LAT imageries, was successfully developed to extract irregular perimeters of 3D grains, their fabric, and their motions (displacements and rotations) caused by loading. This micromechanical information together with the overall behavior of the granular assemblage, such as stress-strain curves and dilatancy characteristics, are quite useful for validating various empirical rules and/or numerical simulations, and also for providing new physical insights in this field.

Key words: image analysis, LAT (laser-aided tomography), micromechanics of granular materials, plane strain compression (PSC) test, visualization (**IGC**: D6)

INTRODUCTION

It has come to be recognized that a granular medium subjected to a localized deformation exhibits non-local (or microstructural) effects. Shear-banding, a typical example, has been intensively discussed through both experimental and theoretical-studies (Muhlhaus and Vardoulakis, 1987; Han and Vardoulakis, 1991; Yoshida et al., 1994). The bearing capacity of ground supporting a footing can be viewed as a non-local effect of shear bands formed just beneath the footing edge (Tatsuoka et al., 1991; Tejchman and Herle, 1999). These examples show that the interaction between micro-macroscopic features of a granular material can be found in a variety of geotechnical problems. This micro-macro interaction is qualitatively understood as the consequence of the presence of a granular cluster (micro structure) in the interior of the entire mass constraining the development of strain localization, thus causing its overall strength to be larger. However, for a quantitative conclusion, a thorough discussion based on precisely observed changes in a granular fabric is necessary.

Rowe (1962) studied some fundamental aspects of the micro-macro interactions by using a pile of two dimensional rods; and this was then followed by further extensive studies by such researchers as Drescher and de Jong (1972), Oda and Konishi (1974), Matsuoka (1974), and Calvetti et al. (1997). In recent decades numerical methods for describing discrete particles (Discrete Element Method (DEM, Cundall and Strack, 1979), for example) have been extensively used to pursue grain-to-grain interactions (Bardet and Proubet, 1991; Rothenberg and Bathurst, 1992; Matsuoka and Yamamoto, 1993; Iwashita and Oda, 1998; Matsushima and Konagai (2001) etc.). These numerical approaches have an advantage in that all the parameters that describe micromechanical features (vectors of grain motions, contact forces etc.) can be tracked throughout the deforming process.

For all the merits of such numerical methods, geotechnical professionals are not always satisfied with numerical results without verification being provided through experiments, because natural sands and gravels made up of arbitrarily-shaped grains often behave quite differently from ideal assemblies of cylinders and/or spheres. On the other hand, it is possible to say that conventional experimental methods provide no micromechanical information from the interior of an opaque specimen.

Some attempts to visualize the interior of a specimen have been made by several researchers. Oda et al. (1972) and Oda and Kazama (1998) used resin to solidify a sand specimen. The specimen was then cut in slices and granular fabrics in its interior were then observed with a microscope. Allesma (1987, 1994) developed a photoelastic technique with a laser light to visualize stress distributions within granular fabrics made up of glass grains. Konagai et al. (1992) developed a method called "Laser-Aided Tomography" (LAT). In this method, a specimen made up of glass grains is optically sliced by a laser-light

[i] Associate Professor, Institute of Engineering Mechanics and Systems, University of Tsukuba, Japan.
[ii] Newjec Corp., 1-15-15, Nishikata, Bunkyo-ku, Tokyo 113-0024 (formerly graduate student, University of Tokyo).
[iii] Professor, Institute of Industrial Science, University of Tokyo, Japan.
Manuscript was received for review on July 11, 2001.
Written discussions on this paper should be submitted before May 1, 2003 to the Japanese Geotechnical Society, Sugayama Bldg. 4F, Kanda Awaji-cho 2-23, Chiyoda-ku, Tokyo 101-0063, Japan. Upon request the closing date may be extended one month.

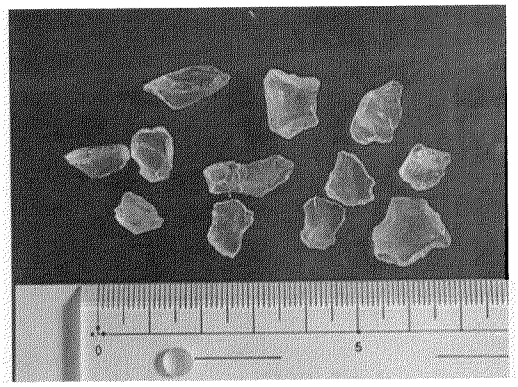

Fig. 1. Crushed glass grains (after grinding)

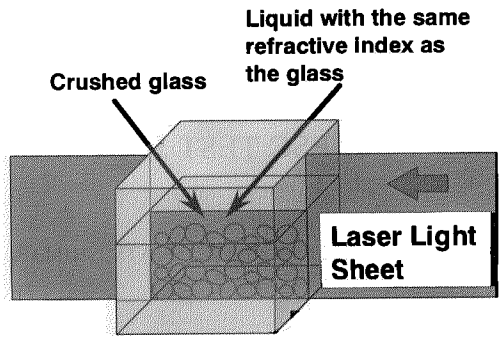

Fig. 2. Diagram of laser-aided tomography

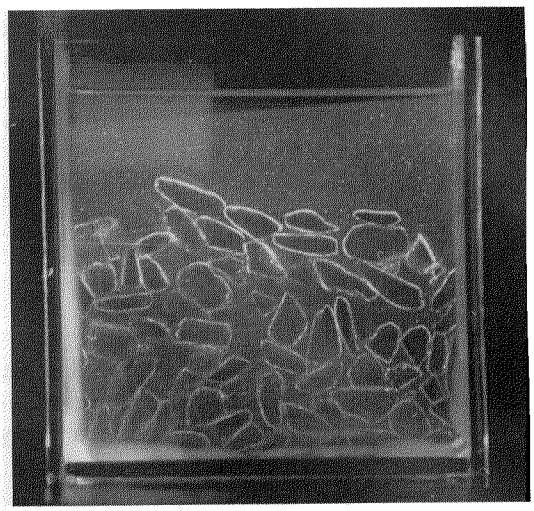

Fig. 3. LAT image

sheet, which enables us to observe each grain motion within the cross section. Desrues et al. (1996) and Otani et al. (2000) succeeded in visualizing 3D void evolutions in a tri-axial test specimen using an X-ray tomography technique. Nakagawa et al. (1999) applied MRI techniques to visualize grains in the interior of their assemblage packed in a sphere by analyzing the orientations of grains from detected contact points.

The Physical Slicing Method (Oda et al., 1972; Oda and Kazama, 1998) has a remarkable advantage in that we can very clearly observe every grain and void; however, it does not provide any information regarding grain motions. Both the X-ray and the MRI methods are highly advanced methods for medical and industrial uses, and various supplemental devices and techniques are commercially available. They, however, allow only indirect observations, and their output values need to be properly transformed into density information.

The methods using a laser require the use of transparent granular materials immersed in a special liquid with the same refractive index so that the specimens are totally transparent. Needless to say, this limitation on materials is clearly a drawback as compared with other methods for testing natural sands and gravels. Moreover, LAT requires that two sides of its specimen (Note: The specimen is box-shaped and there are 6 sides (or surfaces)) must be made transparent to let a laser light travel through and to observe the cross section; but, it does have the great advantage of allowing direct observations of the 3D granular fabrics in real time. Additionally, contact-force magnitudes can be visualized when the specimen is put in a polari-scope arrangement (Allesma, 1987, 1994). Matsui et al. (2001) also showed the potential of this type of method by visualizing pore water flows.

This paper attempts the quantification of a 3D granular fabric made up of irregularly-shaped grains using the LAT technique. A newly developed technique for processing LAT imageries containing a large number of grains is described first. Secondly, the latter half of this paper, describes a special setup for Plane Strain Compression Tests with the LAT visualization technique implemented (PSC/LAT setup), and demonstrates that the PSC/LAT setup allows microscopic views of interior grains (displacements and rotations) to be quantitatively discussed in connection with the macroscopic (overall) behavior of the specimen.

LAT: LASER-AIDED TOMOGRAPHY

A granular model for the LAT test is made up of crushed optical glass grains (Fig. 1). The model is then submerged in a mixture of two silicon oils with its refractive index tuned exactly to that of the glass to make the model totally transparent and invisible. An intense laser light sheet then passes through the specimen, illuminating contours of all grains on the optically cut cross section (Figs. 2 and 3). Scanning the model with the Laser light sheet thus allows the 3D image of every grain in the granular fabric to be visualized.

Crushing glass block is, for the present, the surest process for producing grains for LAT experiments. The fresh surface of a broken glass piece is chemically active, and changes its refractive index slightly from its pre-crushed state. Glass grains produced through a melting process often contain entrapped air bubbles, and therefore are not suited for LAT experiments.

Crushed glass grains are more angular than natural sands and gravels (Konagai, 1999), and they are ground

by a ball-mill to reduce their angularities. Figure 1 shows the grains after 12 hours of grinding.

Since the refractive index of the liquid for immersion varies with temperature, it is essential to minimize room temperature fluctuations.

LAT has mainly been applied to small-scale model tests such as dynamic slope stability experiments and bearing capacity tests (Konagai et al., 1992; Konagai et al., 1994; Matsushima et al., 1996), and has successfully provided 3D images of dynamically changing granular fabrics. The discussions on LAT 3D imageries, however, have been rather qualitative because of the lack of an appropriate image-processing tool. The newly developed algorithm for the LAT image processing follows hereafter.

LAT IMAGE PROCESSING

Present Edge-Detection Scheme

In LAT experiments, edges of all grains on an optically cut cross-section appear as bright lines of diffused laser light. Detecting the grain edges is, however, not easily done for the following reasons:

(1) Grain shapes in LAT experiments are noticeably irregular because grains are produced by crushing a glass block. If each grain shape is simple and regular, there are a variety of accurate and efficient algorithms already available in the field of image processing.

(2) Since only grain contours are illuminated in LAT, it is difficult to distinguish grains automatically from the surrounding voids.

(3) A contour of a grain touches those of neighboring grains. Therefore, when the contour line is tracked stepwise, it is very easy to take a wrong path at these points of contact.

Taking into account these features producing difficulties for LAT imagery, a semi-automatic graphical users interface (GUI) has been developed, which allows for a man-computer interactive operation in which an operator identifies a grain by clicking three points (Points A, B and C in Fig. 4) so that the line segments AB and AC indicate the long axis and short axis of the grain, respectively. Then the edge line is tracked counterclockwise from Half-line AB. The variation of green laser light intensity with a radial distance r (Half-line AD in Fig. 4) is given by $f(r)$ (The argon-ion laser used in the LAT experiments emits several monochromatic lights by adjusting the orientation of a built-in prism, with the green light (514.5 Å) being the most intense). In addition to $f(r)$, two weighing functions, $g(r)$ (=rectangular window) and $h(r)$ (=limiter) are introduced (*see* Fig. 4).

$$g(r)=\begin{cases}1 & ((1-\alpha)r_p \le r \le (1+\alpha)r_p)\\ 0 & (r<(1-\alpha)r_p,\ r\ge(1+\alpha)r_p)\end{cases}$$

$$h(r)=\begin{cases}1 & (0\le r\le AD)\\ 1-\beta(r-AD) & (r>AD)\end{cases}$$

where r_p is the mid point of the rectangular $g(r)$ window opening, which is set at the radial distance detected in the previous search, and $2\alpha r_p$ is the opening of the window. To realize the continuity between the edge points, $g(r)$ is introduced.

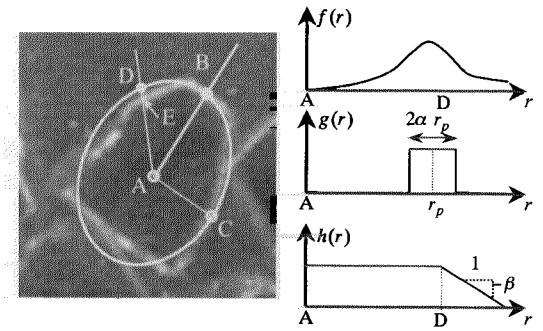

Fig. 4. Present edge-detection algorithm

The limiter $h(r)$ decreases linearly at a constant rate of $dh/dr=-\beta$ as the radial distance r increases beyond Point D in Fig. 4, which avoids the tracked edge line diverging from the ellipse defined by Points A, B and C.

Using these functions, the edge point (Point E in Fig. 4) along Half-line AD is determined so that $AE=r_e$ where r_e satisfies

$$f(r)\cdot g(r)\cdot h(r) \quad \text{maximum.}$$

Parameters α and β were set at 0.1 and 1.0, respectively, by trial and error. Though some manual corrections through GUI are still necessary, the present algorithm allows grain edges to be quickly tracked.

Resolution of the Analysis

Accuracy of the edge detection is greatly affected by the quality of LAT images. The quality of LAT imagery is dependent on the sharpness of the laser sheet that optically cuts the model in half. Since the laser light sheet is about 0.5 mm to 1.0 mm thick in the present experiment, grains finer than this thickness cannot be detected. Air bubbles and dust caught in the model also deteriorate the quality of the LAT image. Imperfect tuning of the liquid's refractive index can also cause vague grain images to be photographed. Despite all the careful manipulations of the above-mentioned conditions, there still remains a maximum 5% error of edge locations in terms of radial distances in the following example.

Example of Edge Detection

Glass grains with diameters ranging from 5.0 mm to 10.0 mm were piled loose in a cubic glass vessel (10 cm by 10 cm by 10 cm). Then a laser light sheet cutting through the model was moved stepwise at every 2 mm interval, and successive LAT images were photographed. Figure 5(b) shows the edges detected from one of the photographed LAT imageries (Fig. 5(a)). Both locations and shapes of grains seem to be detected with sufficient accuracy.

With this digital data, various properties for describing this granular fabric can be directly calculated. The void ratio for this particular cross-section (Fig. 5(b)) can be

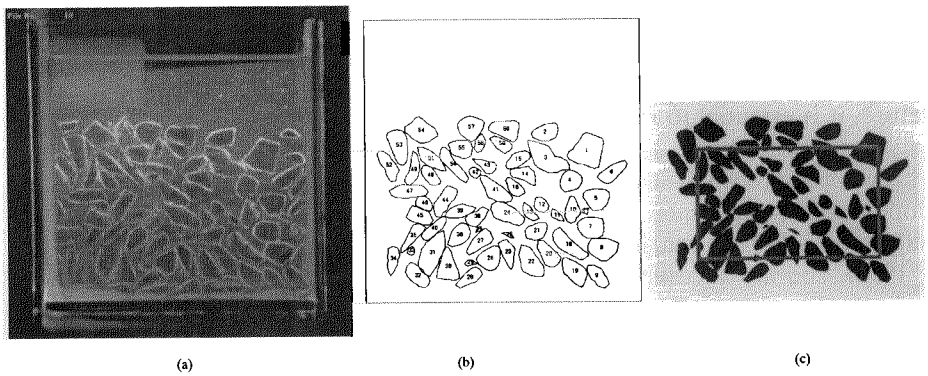

(a) (b) (c)

Fig. 5. An example of edge detection: (a) an original LAT image, (b) result of edge detection and (c) void ratio calculation

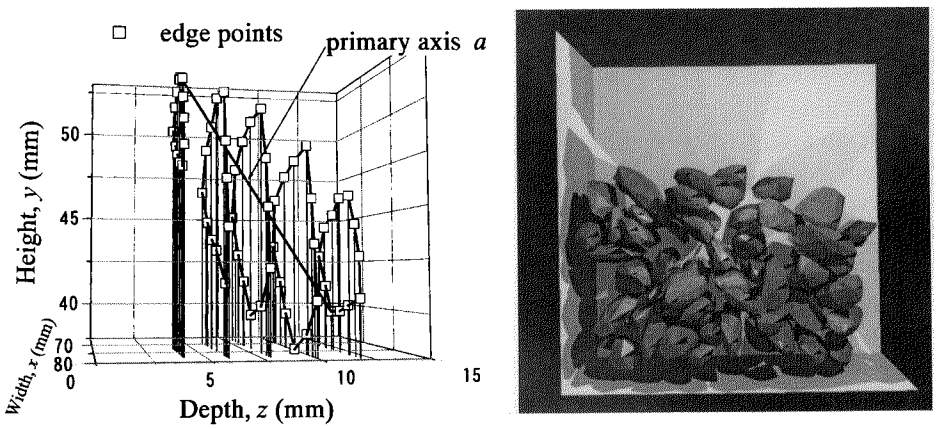

(a) (b)

Fig. 6. 3D grains reconstructed from LAT images: (a) integration of the edges for a 3D grain image and (b) 3D grains intersecting a specific cross section

easily calculated by counting the pixels included in the voids, and is found to be 0.728.

Stacking up the cross-sections with the detected edge of a particular grain, a 3D image of the grain is obtained as shown in Fig. 6(a). Applying this process to all other grains that intersect a specific cross section, the 3D image of the granular fabric appears as shown in Fig. 6(b).

3D grain shape parameters can be obtained as follows. The primary principal axis, a, is obtained by searching for a pair of points on the grain surface which makes the distance between these two the longest (Fig. 6(a)). The secondary principal axis, b, is then obtained by searching for pairs of those points furthest from each other in all cross-sections orthogonal to the primary long axis a. Finally the third axis, c, which is orthogonal to both a and b, is obtained (Fig. 7(a)). Figure 7(b) shows the spatial distribution of a and b for all the grains shown in Fig. 6(b). It is noted that most of the secondary principal axes b fall in the range of the diagonal openings of the sieves ($5\sqrt{2}$ to $10\sqrt{2}$ mm). Figure 7(c) shows the spatial orientations of the longest axes a.

LAT/PSC TEST

As has been mentioned, it is essential in the study of mechanical features of a granular assemblage that due attention is paid to both microscopic behaviors (grain-to-grain interactions) and macroscopic features. For this, a Plane Strain Compression (PSC) testing apparatus with a supplement for LAT visualization was set up as shown in Figs. 8 and 9. The setup is a very simple assembly of minimum essentials. Without a pressure cell, the confining pressure is provided by vacuuming the specimen. A transparent acrylic pedestal was put at the bottom end of the specimen so that the laser light sheet can travel up through the model from the bottom. The front side of the specimen must be made transparent to observe the interior of the specimen. Since a completely transparent membrane that can stretch and contain angular grains is not commercially available as an industrial product, one side of the rubber membrane covering the specimen was cut open in a rectangular fashion, and the four sides of the opening were pinched in between two acrylic plates, the inner plate contacting the grains directly. However, this setup causes a relatively large friction to be induced between the grains and the inner acrylic plate, thus dis-

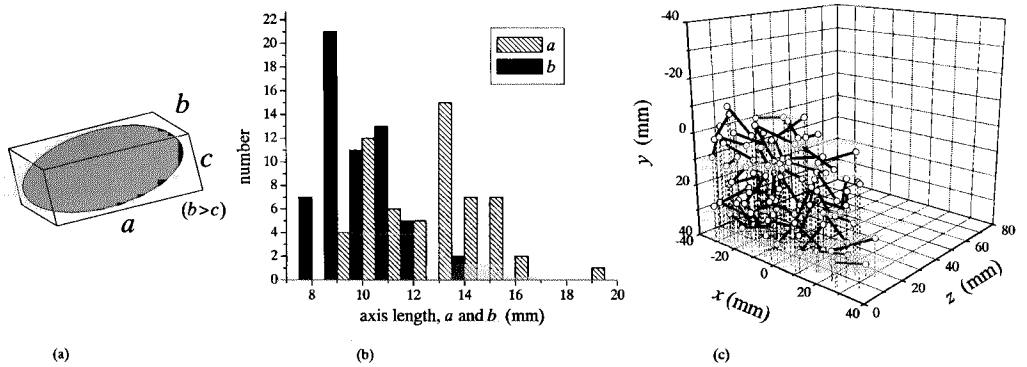

Fig. 7. Statistics of grain shape and the orientation of grains obtained by LAT image analysis: (a) the axes *a*, *b* and *c* of a grain, (b) distribution of *a* and *b* and (c) spatial distribution of *a*

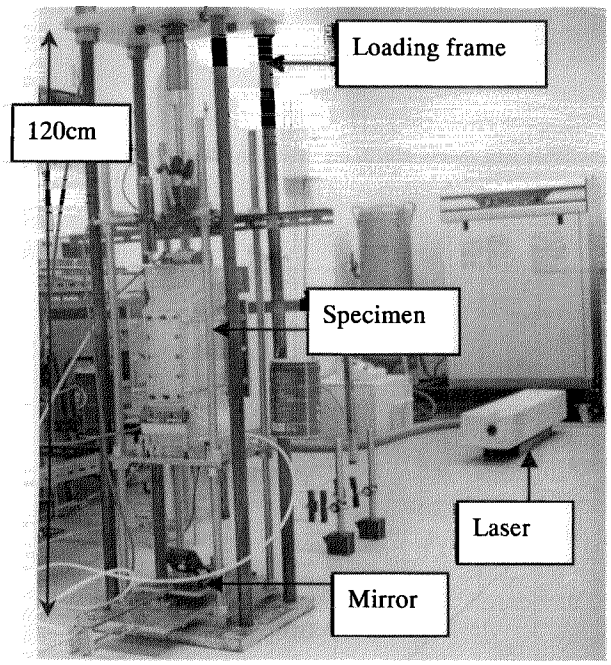

Fig. 8. LAT/PSC apparatus

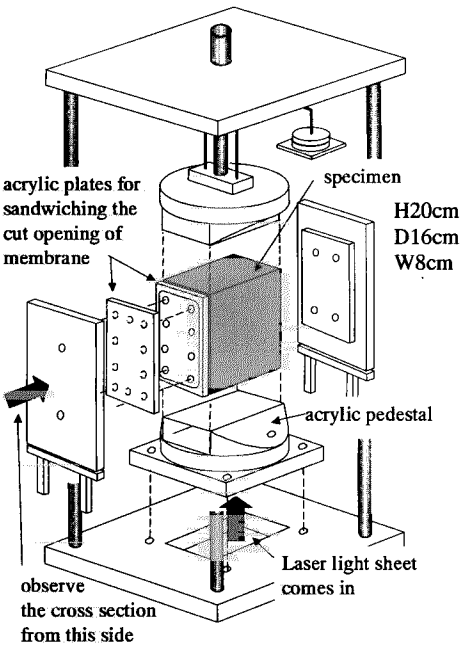

Fig. 9. Diagram of LAT/PSC system

turbing stress distribution near the plate. This problem was not solved in the present experiment, but replacing the acrylic plate with a very hard glass plate may improve the situation.

A dense specimen (H20 cm × D16 cm × W8 cm) was prepared by pluviating poorly-graded grains (D_{50} = 7.3 mm) through air. After letting CO_2 gas permeate through the specimen for hours, the mixture of two silicon oils used for immersion gradually percolated up through the specimen. Then axial strain was given at a steady rate of 0.228%/min under the constant confining pressure of 78 kPa = 0.8 kgf/cm^2. The subsequent testing procedured used followed the example specified by Tatsuoka et al. (1994).

TEST RESULTS AND DISCUSSION

Macro Behavior

Figures 10(a) and (b) show the overall deviator stress vs. axial strain, and volumetric strain vs. axial strain relationships, respectively, from a drained compression test. The stress-strain curve is very jaggy, which often happens when grains are not sufficiently small in comparison with the dimensions of a specimen. The peak friction angle ϕ_{peak} of 56 degrees was reached for this very angular granular assemblage, and the maximum dilatancy angle, $\nu_{d,max}$, of about 22–23 degree was also very high. It is however noted that the measure of inter-particle friction, $\phi_{peak} - \nu_{d,max}$, was about 33–34 degree, and is comparable with that of a natural sand (Tatsuoka et al., 1994; Yoshida, 1994).

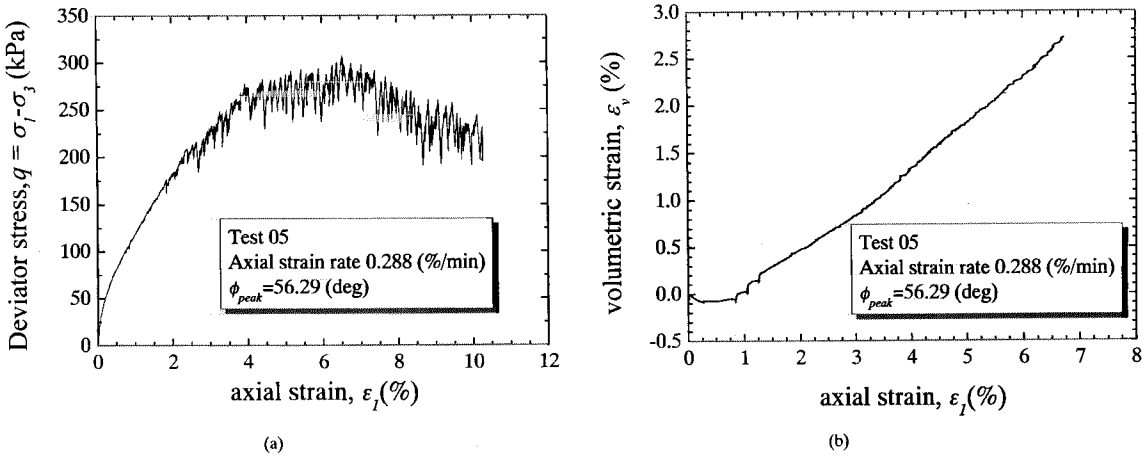

Fig. 10. Global response of LAT/PSC test: (a) stress-strain relationship and (b) dilatancy relation

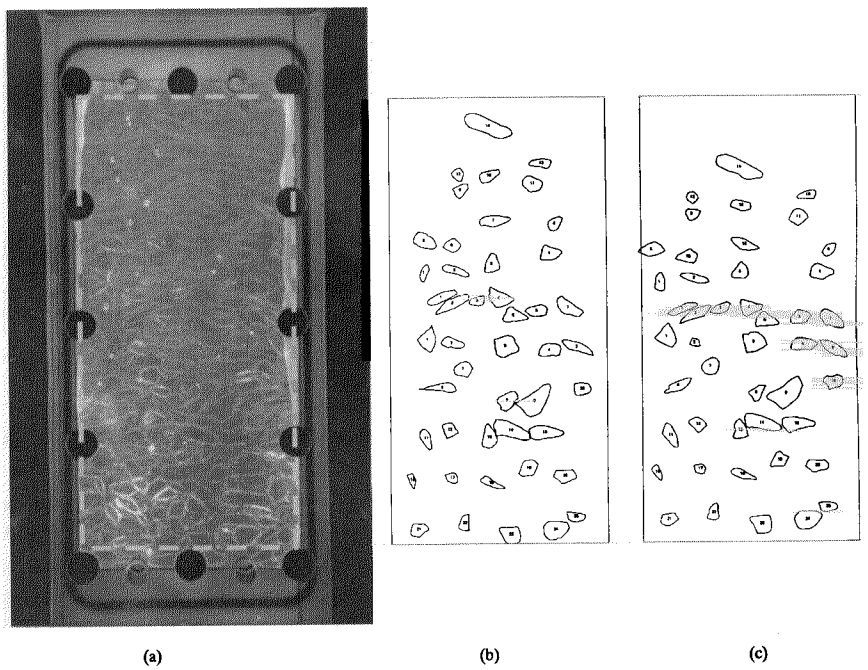

Fig. 11. Contours of representative grains: (a) LAT image, (b) initial state and (c) residual state

Grain Motion

Figure 11(a) shows a LAT image photographed from the front side of the specimen before axial load was applied. The laser light sheet cut the specimen at about 3 cm behind its front surface. A total of 46 grains were taken as targets (Fig. 11(b)), and their shapes and motions were tracked using the above-mentioned image-processing technique. Figure 11(c) shows the target grains remaining on the laser light sheet when a macro axial strain of 10.3% was reached. The fact that all target grains remained on the same plane at the same depth indicates that the grains did not move a lot in the σ_2 direction of the specimen. Taking this fact into account, the following discussion is based on the images from this particular cross-section, ignoring out-of-the plane motions and associated rotations.

Figure 12(a) shows the displacements of the grains' centroids, major axes and rotations obtained from Figs. 11(b) and (c). The target grains rotate remarkably. The more upper the grains are located, the larger the rotation angles. From the displacements of the grains centroids, deformation of the cross-section was calculated (Fig. 12(b)). In this calculation the nearest six grains are taken to adjust coefficients of a polynomial for describing the induced displacement field in the least square sense. The calculated shape of the deformed specimen seems to agree well with its photographed shape (Fig. 12(c)).

It is noted that the displacement field obtained here is considered as a macro kinematic field. The Mindlin's micro-structured continuum (Mindlin, 1964) requires additional kinematic variables that describe the micro-rotational term as well as the micro-stretching term. The

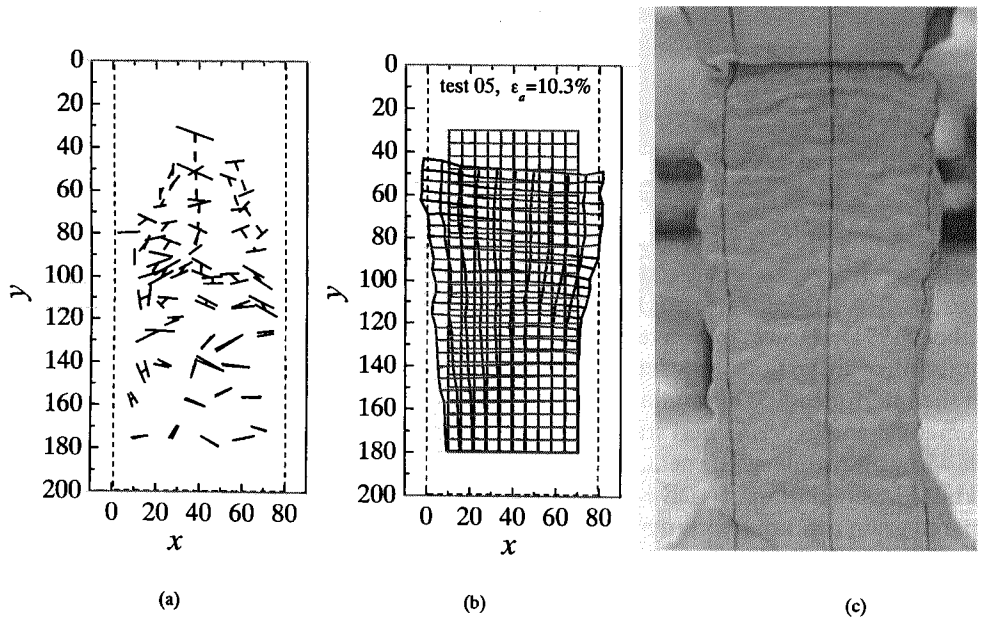

Fig. 12. Deformation of specimen: (a) displacement and rotations of the grains, (b) deformation pattern calculated from (a) and (c) deformed specimen

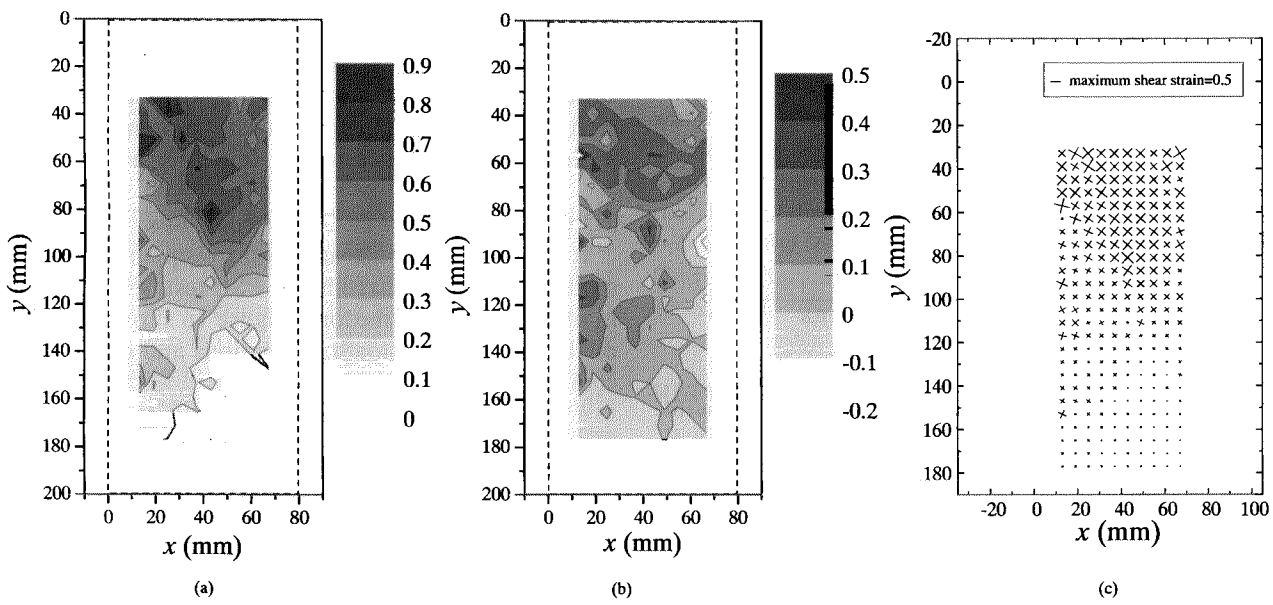

Fig. 13. Strain distributions: (a) maximum shear strain, (b) volumetric strain and (c) direction of maximum shear strain

former is interpreted as the rotation of a grain in a granular fabric, while the latter describes the deformation of the grain. However, the latter is often ignored (Muhlhaus and Vardoulakis, 1987; Chang and Ma, 1991) because its effect is less important than the grain's rotation.

Local Strain Field

From the observed displacement field, spatial distribution of strain is directly calculated. Figures 13(a) and (b) show distributions of the maximum shear and volumetric strains, γ_{max} and ε_v, respectively, and Fig. 13(c) shows the directions of maximum shear strains at all nodes. It is recognized from these figures that a narrow band of localized strain slants diagonally downward-to-the-right and dies out as it goes further down. Figure 14 shows the relationship between γ_{max} and ε_v at all nodal points together with the overall relationship (solid line in Fig. 14). Though the points scatter remarkably, their regression curve, the third-order polynomial through these points, agrees well with the overall relationship before the peak strength is reached ($\gamma_{max}<0.2$). Note that the strain is considered to be uniformly distributed, and thus the overall relationship reflects the microscopic relationship before the shear band develops.

Relation between Grain Rotation and Continuum Rota-

tion

The role of grain rotation in a granular fabric is still a controversial problem. When spherical grains with no surface friction are packed together, each grain's rotation has no effect on the overall behavior. As for a real granular material, however, the rotation of a grain is transmitted to the surrounding grains, and its effect has been discussed in contrast to continuum rotation. Actually, the gradient of rotation is an important key parameter in the Cosserat continuum (Muhlhaus and Vardoulakis, 1987; Bardet and Proubet, 1991). However conventional experimental methods offer little potential for observing grain rotations in the interior of a 3D granular assembly, and only a few numerical and experimental studies on 2D models have dealt with this problem. Bardet and Proubet (1991) conducted a DEM simulation of a 2D biaxial loading test and compared grain rotations within a shear band with the corresponding rotations of the continuum. Their result showed that grains in the shear band rotated about twice as much as the corresponding rotation in the continuum. Calvetti et al. (1997) conducted a series of experiments with circular rods, and observed that the average grain rotations in pure compression and simple shear are very close to the continuum rotation, excluding those cases under more complicated loadings.

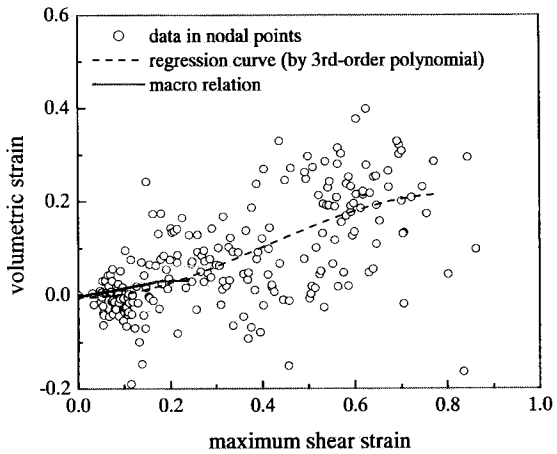

Fig. 14. Relation between maximum shear strain and volumetric strain

By virtue of the LAT potential for visualizing 3D granular fabric, the spatial distribution of grain rotation, $\theta_G = \theta_G(x, y)$ was calculated from the visualized major axes of the grains (Fig. 12(a)) and is shown in Fig. 15(a); Fig. 15(b) contrasts the corresponding rotations, θ_C, in the continuum calculated from the following rigid rotation tensor $\boldsymbol{R}$ (for examples *see* Bardet and Proubet, 1991):

$$\boldsymbol{R} = \begin{bmatrix} \cos\theta_C & \sin\theta_C \\ -\sin\theta_C & \cos\theta_C \end{bmatrix} = \boldsymbol{V}^{-1}\boldsymbol{F}$$

where $\boldsymbol{V}$ is the left stretch tensor (symmetric) and $\boldsymbol{F}$ is the (macro) deformation gradient. It is worth emphasizing that this continuum rotation was calculated only from the displacements of the grain centroids, and does not include the information of grain rotations.

In general, distributions of both θ_G and θ_C exhibit a similar pattern in which negative values (clockwise rotations) appear mostly in the zones of localized strain. However, the grain rotations are much bigger than the continuum rotations. For further, more extensive discussions, this result will have to await comparisons with the authors' experiments on some smaller grains.

3D Grain Motion in PSC Test Specimen

It is worth demonstrating that even under the plane strain condition realized in the PSC test, grains can move in all 6 degrees of freedom. Figure 16 shows an example of the pre and post-loading locations and orientations of some target grains, among others.

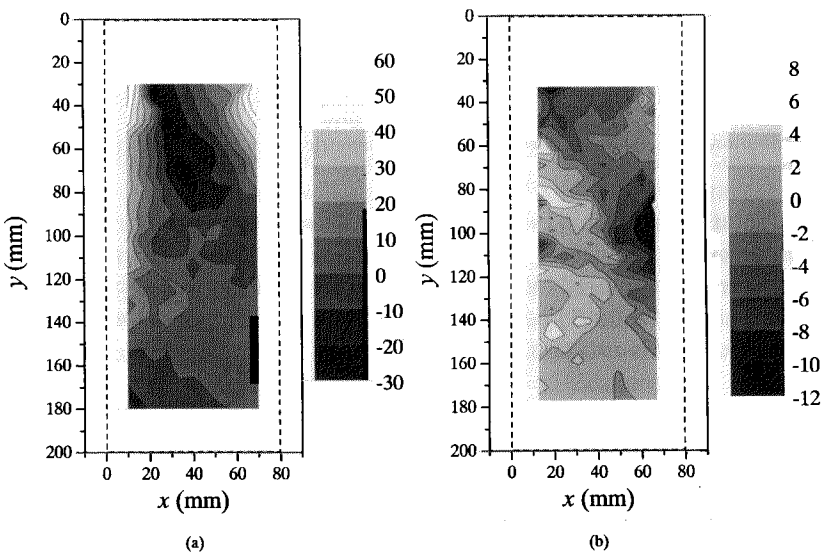

Fig. 15. Distribution of grain rotation and continuum rotation: (a) grain rotation θ_G (deg.) and (b) continuum rotation θ_C (deg.)

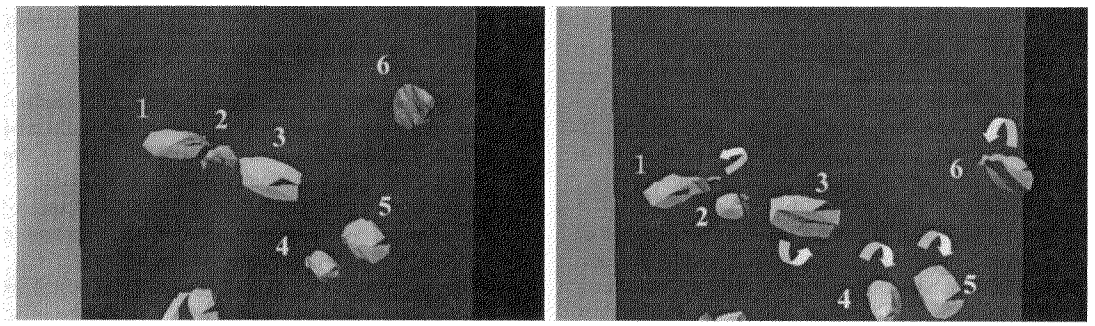

Fig. 16. 3D grain rotation inside PSC specimen

CONCLUSIONS AND REMAINING TECHNICAL PROBLEMS

This paper demonstrated that the present LAT/PSC testing method offers the potential for discussing micro and macro mechanics of granular structures with visualized 3D images of granular fabrics. Though the method limits the grains for the experiment to completely homogeneous and transparent ones, the visualized LAT imagery allows both the 3D shapes of grains and their motions in 6 degrees of freedom to be thoroughly analyzed, which the great advantage featured in this method in contrast to existing visualization techniques. However, the following points should be improved for more credible results:

(1) Sharpness of LAT imageries
The accuracy of the image processing of 3D granular fabrics depends strongly upon the quality of the photographed LAT imageries. This problem becomes more serious as the grain size decreases. There are two major causes for deterioration of the photo quality in the LAT/PSC tests: tiny entrapped air bubbles and imperfect tuning of the liquid's refractive index to that of the glass grains. The former can be greatly improved by using a pressure cell so that larger negative pressure can be applied to the specimen to suck the bubbles out of the specimen before loading. The latter problem depends upon various details for the tuning processes, but strict control of the room temperature will certainly help to improve it.

(2) Grain-edge detection algorithm
As already described, the present algorithm is not completely automatic, and requires some manual, by eye, corrections. This procedure requires a lot of time and effort as the number of grains increases, and errors may not stay within acceptable tolerances. Development of a fully automatic algorithm based on more advanced technology is thus indispensable for more efficient image-processing.

(3) Production of glass grains
Crushed glass grains have very angular shapes as contrasted with natural sands and gravels. Though grinding the glass grains in a ball-mill improves their shapes, it does not to a satisfactory extent. Thus, some more efficient ways have to be realized.

(4) Friction between glass grains and the acrylic window panel (σ_2-plane)
Since the glass grains are harder than the acrylic window panel, angular glass grains scratch the plate causing friction on the interface to be remarkably increased. To minimize this effect, the acrylic window panel can be replaced with a hard glass plate, and some lubricant used.

ACKNOWLEDGMENTS

The authors wish to thank Prof. Fumio Tatsuoka, University of Tokyo, for invaluable advice and discussion. The authors are also grateful to Mr. Sato, University of Tokyo, for his help in developing the LAT/PSC apparatus. Partial financial supports for this study have been provided by the Ministry of Education, Science and Culture (Grant in Aid for Scientific Research, No. 12355020).

REFERENCES

1) Allesma, H. G. B. (1987): Optical analysis of stress and strain in photoelastic particle assemblies, *Doctor thesis*, Delft University of Technology.
2) Allesma, H. G. B. (1994): Using image processing in analyzing stresses in photoelastic granular material, *Proc. 10th Int. Conf. on Experimental Mechanics*, Lisbon, 113-118.
3) Bardet, J. P. and Proubet, J. (1991): A numerical investigation of the structure of persistent shear bands in granular media, *Géotechnique*, **41** (4), 599-613.
4) Calvetti, F., Combe, G. and Lanier, J. (1997): Experimental micromechanical analysis of a 2D granular material: relation between structure evolution and loading path, *Mech. Cohesive-Frictional Materials*, **2**, 121-163.
5) Chang, C. S. and Ma, L. (1991): A micromechanical-based micropolar theory for deformation of granular solids, *Int. J. Solids Structures*, **28** (1), 67-86.
6) Cundall, P. A. and Strack, O. D. L. (1979): A discrete numerical model for granular assemblies, *Géotechnique*, **29** (1), 47-65.
7) Desrues, J., Chambon, R., Mokni, M. and Mazerolle, F. (1996): Void ratio evolution inside shear bands in triaxial sand specimens studied by computed tomography, *Géotechnique*, **46** (3), 529-546.
8) Drescher, A. and de Jong, G. J. (1972): Photoelastic verification of a mechanical model for the flow of a granular material, *J. Mech. Phis. Solids*, **20**, 337-351.
9) Han, C. and Vardoulakis, I. (1991): Plane-strain compression experiments on water-saturated fine-grained sand, *Géotechnique*, **41**

(1), 49–78.
10) Iwashita, K. and Oda, M. (1998): Rotational resistance at contacts in the simulation of shear band development by DEM, *J. Eng. Mech. Div.*, **124** (3), ASCE, 285–292.
11) Konagai, K., Tamura, C., Rangelow, P. and Matsushima, T. (1992): Laser-aided tomography: A tool for visualization of changes in the fabric of granular assemblage, *Structural Engrg./Earthquake Engrg.*, JSCE, **9** (3), 193s–201s.
12) Konagai, K., Matsushima, T. and Sato, T. (1994): Dependence on frequency of dynamic inter-particle dislocation within a slope, *Structural Engrg./Earthquake Engrg.*, JSCE, **11** (2), 93s–101s.
13) Konagai, K. (1999): Visualization of fabric by laser-aided tomography, *Mech. of Granular Materials: An Introduction* (eds. by Oda, M. and Iwashita, K.), A.A. Balkema, 248–257.
14) Matsui, G., Mishiro, K., Monji, H., Tanaka, M. and Kamide, H. (2001): Flow characteristics in channel with local blockage packed with spheres, *Proc. 5th World Conf. on Experimental Heat Transfer, Fluid Mechanics and Thermodynamics* (eds. by Celata et al.), 1675–1682.
15) Matsuoka, H. (1974): A microscopic study on shear mechanism of granular materials, *Soils and Foundations*, **14** (1), 29–43.
16) Matsuoka, H. and Yamamoto, S. (1993): A microscopic study on shear mechanism of granular materials by DEM and experiments, *Powders and Grains 93, Proc. Second Int. Conf. on Micromechanics of Granular Media* (ed. by Thornton, C.), 155–160.
17) Matsushima, T., Date, K., Katagiri, T. and Konagai, K. (1996): Effect of negative excessive pore pressure on the dynamic stability of submerged granular slope, *Bull. ERS*, (29), 13–24.
18) Matsushima, T. and Konagai, K. (2001): Grain-shape effect on peak strength of granular materials, *Proc. 10IACMAG: The 10th Int. Conf. Computer Methods and Advances in Geomechanics*, **1**, 361–366.
19) Mindlin, R. D. (1964): Microstructure in linear elasticity, *Arch. Rational Mech. Anal.*, **16**, 51–78.
20) Muhlhaus, H.-B. and Vardoulakis, I. (1987): The thickness of shear band in granular materials, *Géotechnique*, **37** (3), 271–283.
21) Nakagawa, M., Waggoner, R. A. and Fukushima, E. (1999): Non-invasive measurement of fabric of particle packing by MRI, *Mechanics of Granular Materials: An Introduction* (eds. by Oda, M. and Iwashita, K.), A.A. Balkema, 240–248.
22) Oda, M. and Konishi, J. (1974): Microscopic deformation mechanism of granular material in simple shear, *Soils and Foundations*, **14** (4), 25–38.
23) Oda, M., Kobayashi, H., Yamazaki, Y. and Onodera, T. (1972): A new technique for determination of void ratio and its variation within deformed granular material, *Report of Depart. Found. Engrg. Fac. Engrg. 3*, Saitama University, 39–50.
24) Oda, M. and Kazama, K. (1998): Microstructure of shear bands and its relation to the mechanisms of dilatancy and failure of dense granular soils, *Géotechnique*, **48** (4), 465–481.
25) Otani, J., Mukunoki, T. and Obara, Y. (2000): Application of X-ray CT method for characterization of failure in soils, *Soils and Foundations*, **40** (2), 111–118.
26) Rothenburg, L. and Bathurst, R. J. (1992): Micromechanical features of granular assemblies with planar elliptical particles, *Géotechnique*, **42** (1), 79–95.
27) Rowe, P. W. (1962): The stress-dilatancy relations for static equilibrium of an assembly of particles in contact, *Proc. Royal Soc. London, Series A*, **269**, 117–141.
28) Tatsuoka, F., Sato, T., Park, C.-S., Kim, Y.-S., Mukabi, J. N. and Kohata, Y. (1994): Measuring of elastic properties of geomaterials in laboratory compression tests, *Geotech. Testing J.*, **17** (1), 80–94.
29) Tatsuoka, F., Okahara, M., Tanaka, T., Tani, K., Morimoto, T. and Siddiquee, M. S. A. (1991): Progressive failure and particle size effect in bearing capacity of a footing on sand, *Proc. Geotech. Engrg. Congress*, ASCE Geotech. Special Publication, (27), 788–802.
30) Tejchman, J. and Herle, I. (1999): A "class A" prediction of the bearing capacity of plane strain footings on sand, *Soils and Foundations*, **39** (5), 47–60.
31) Vardoulakis, I. and Graf, B. (1985): Calibration of constitutive models for granular materials using data from biaxial experiments, *Géotechnique*, **35** (3), 299–317.
32) Yoshida, T. (1994): Strain localization and shear banding during failure of sands, *Doctor thesis*, University of Tokyo (in Japanese).
33) Yoshida, T., Tatsuoka, F., Siddiquee, M. S. A., Kamegai, Y. and Park, C.-S. (1994): Shear banding in sands observed in plane strain compression, *Proc. Symp. on Localization and Bifurcation Theory for Soils and Rockes* (eds. by Chambon et al.), Balkema, 165–179.